



# Tuning physical, mechanical and barrier properties of cellulose nanofibril films through film drying techniques coupled with thermal compression

Ikramul Hasan · Jinwu Wang · Mehdi Tajvidi

Received: 14 July 2021 / Accepted: 13 October 2021 / Published online: 31 October 2021  
© The Author(s), under exclusive licence to Springer Nature B.V. 2021

**Abstract** Cellulose nanofibrils (CNFs) have already been proved to be a potential candidate as one of the next-generation renewable and sustainable packaging materials. However, the mechanical and barrier properties of CNF films are not yet up to the mark for certain applications, especially at higher relative humidity. Those properties can be controlled by the degree of fibrillation of fibers and drying methods of films. Here we prepared CNF films from CNF suspensions with two different degrees of fibrillation—standard CNF (90% fine) and high-fine CNF (97% fine) by casting and filtration. These were dried in four different ways (air, oven, heat gun, and hot press drying) to better understand how these methods affect the physical, mechanical as well as oil, water vapor and oxygen barrier properties of the films. The CNF

films made by hot press drying showed the highest tensile strength (98.82 MPa) and lowest water vapor permeability (13.91 g.mm/m<sup>2</sup> day kPa). Hot press compaction on the dried films further improved the tensile strength by 13.1% and reduced the water vapor and oxygen permeability by 22.3% and 43%, respectively. The average value of oxygen permeability after hot press compaction was found to be 403.2 cc μm/m<sup>2</sup> day atm, which can be considered as high oxygen barrier at 80% relative humidity. All prepared films showed maximum oil resistance value with kit number ‘12’, regardless of their preparation techniques. The result of folding a representative CNF film showed that the CNF film retained its oxygen barrier properties after a single line folding, but failed after two crossline folding.

---

**Supplementary Information** The online version contains supplementary material available at <https://doi.org/10.1007/s10570-021-04269-9>.

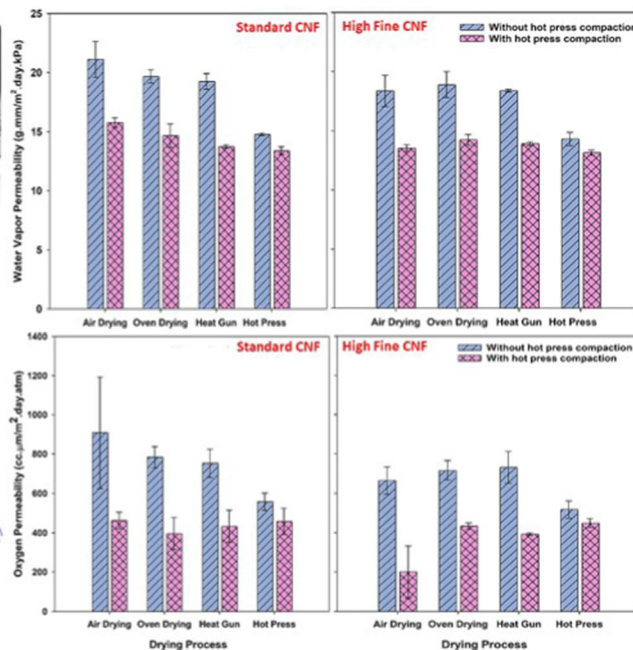
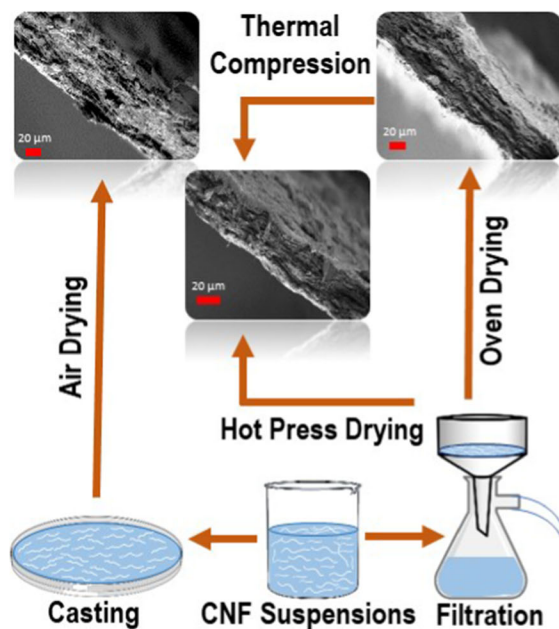
---

I. Hasan · M. Tajvidi (✉)  
School of Forest Resources, University of Maine, 5755  
Nutting Hall, Orono, ME 04469, USA  
e-mail: mehdi.tajvidi@maine.edu

I. Hasan · M. Tajvidi  
Advanced Structures and Composites Center, University  
of Maine, 35 Flagstaff Road, Orono, ME 04469, USA

J. Wang  
Forest Products Laboratory, U.S. Forest Service, 1 Gifford  
Pinchot Drive, Madison, WI 53726, USA

## Graphic abstract



**Keywords** Cellulose nanofibril films · Water vapor permeability · Oxygen permeability · Renewable packaging · Hot pressing · Drying processes · Crack resistance

## Abbreviations

CNF	Cellulose nanofibril
CNC	Cellulose nanocrystal
PVC	Polyvinyl chloride
AFM	Atomic force microscopy
SU	Sheffield Unit
XRD	X-ray diffraction
CI	Crystallinity Index
SEM	Scanning electron microscopy
WVTR	Water vapor transmission rate
WVP	Water vapor permeability
OTR	Oxygen transmission rate
ANOVA	Analysis of variance

## Introduction

Traditional petroleum-based polymers e.g. polyethylene, polypropylene, polyethylene terephthalate, etc.

are used mostly for current packaging applications and have already made our environment polluted from land to ocean (Groh et al. 2019). Although these plastics are cheap, they have some technical limitations as well to ensure the food quality inside them. Polyethylene and some other common plastics provide low water vapor permeability, but fail to restrict higher oxygen transmission (Wang et al. 2018). To increase the shelf life of many types of food, lower oxygen permeability is required to avoid oxidation or any sort of chemical modification of food items inside the package. Polyvinylidene Chloride is a commercial plastic with both good oxygen and water vapor barrier properties. However, it should be avoided due to its release of harmful dioxins when incinerated after use (Wang et al. 2018). One of the most promising alternatives to traditional petroleum-based packaging materials is cellulosic nanomaterials, which have received a lot of attention from researchers around the world due to their high oxygen barrier properties, biodegradability and renewability (Satam et al. 2018; Chowdhury et al. 2019a; Wang et al. 2020).

Cellulose is the most abundant natural polymer on Earth. The primary sources of cellulose are cell walls

of different plants, some algae and bacteria. Cellulose is mostly known for its application in pulp, paper and textile industries. However, when the dimension of cellulose fibers are turned into nanosize (1–100 nm), it finds applications as coatings (Chowdhury et al. 2019b), additives (Fu et al. 2017), binders (Tayeb et al. 2018), electrochemical and piezoelectric materials (Tayeb et al. 2019), analytical systems (Hossen et al. 2020a), biomedical components (Du et al. 2019) and many others yet to explore. The main reasons for those applications of cellulose nanomaterials are the high mechanical strength, low density, good thermal stability, higher transparency as well as renewable and sustainable nature of the material itself (Moon et al. 2016).

Cellulosic nanomaterials are considered to be very good barrier materials for oxygen at lower relative humidity. This can be attributed to the self-assembly between nanofibrils or nanocrystals via the strong hydrogen bonding between -OH groups present in cellulose structure, which eventually makes a film of low porosity to restrict the passage of oxygen molecules (Sacui et al. 2014). Cellulose nanofibrils (CNFs) are considered better barrier materials than cellulose nanocrystals (CNCs) in the absence of orientation as they form a less porous network through entanglement inside the film making a more tortuous path for oxygen movement (Chowdhury et al. 2019b). However, the oxygen barrier property of CNFs drastically decreases at higher relative humidity turning it into a major challenge for the commercialization of CNF based packaging materials (Wang et al. 2020). The main cause of failure at higher relative humidity can be attributed to the absorbance of water molecules into the film at higher relative humidity, which works as a medium for oxygen diffusion through the film and subsequent swelling of the film (Aulin et al. 2010).

CNF films are produced either by casting or filtration followed by a drying process (Aulin et al. 2010; Amini et al. 2020). In casting, the suspension of CNFs at a certain concentration is poured into a container, usually a petri dish, and then dried at a low temperature (around 25 °C), which usually takes more than 24 h for complete drying (Mashkour et al. 2014). On the other hand, filtration is performed in a vacuum or over pressure on a filter paper and then the wet mat can be dried with or without filter paper in any drying apparatus, usually, an oven which takes a maximum of

24 h (Amini et al. 2020; Ghasemi et al. 2020). Fast and efficient drying of CNF films are absolutely necessary for economic production and controlling the properties of the resultant films (Nadeem et al. 2020).

Qing et al (2015) prepared films from three different CNF types and dried them using five different drying methods involving casting, oven drying and freeze drying and studied the changes in mechanical properties of all the produced films and found significant differences in tensile strength and modulus among drying methods. Fein (2021) studied how cast films and filtered films vary in structure as well as mechanical and barrier properties. However, there is no systematic study still available to understand how different drying methods affect the oxygen and water vapor barrier properties of CNF films. There is evidence from other studies that shows drying techniques can control the barrier properties of CNF films. Osterberg et al. (2013) reported the preparation of CNF film within the shortest period of time (1–2.5 h) with hot press drying at 100 °C after filtration and found significantly lower oxygen permeability even at higher relative humidity. Later Tayeb and Tajvidi (2020) prepared oven-dried CNF films which had extremely high value of oxygen transmission rate causing a failed test. When these films were subjected to a simple hot pressing at 130 °C for 1 h, the oxygen transmission rate at 90% relative humidity was significantly reduced to 21.16 cc/m<sup>2</sup> day. However, the effect of hot-press compaction on other drying methods and structural reason behind the decrease in oxygen permeability was not clear from that study.

In this work, we focused to study how different drying processes affect the barrier properties of CNF films, particularly water vapor and oxygen barrier, along with mechanical properties. The overall plan of the study is shown in Fig. 1. Here we prepared films from two different CNF types with different degrees of fibrillation and prepared films by casting and filtration. Besides air and oven drying, we also employed heat gun assisted drying (termed as ‘heat gun drying’ in this paper), which is basically impinging wet films with a hot air jet. The advantage of the hot air jet is that it will shorten the drying time as the following dry hot air will remove the preceding air jet which is already saturated by the moisture released from the wet film. We also used hot pressing as a drying method, which is expected to give dry film within the shortest time

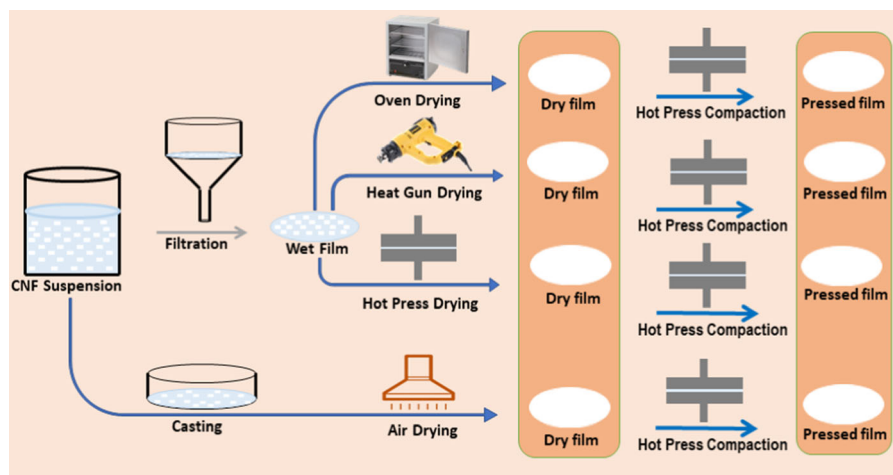


**Fig. 1** Schematic diagram of film preparation and drying techniques used in this study

possible with high mechanical property (El Awad Azrak et al. 2019). Besides hot pressing as a drying method, we also performed hot pressing on all dried films as that may further increase the water and oxygen barrier property as higher relative humidity as suggested by Tayeb et al (2020). This post-processing technique is termed hot press compaction in this manuscript.

## Materials and methods

### Materials

The CNF suspension for this work was provided by the Process Development Center (PDC), University of Maine. The PDC produced the CNF suspension from northern softwood kraft pulp with a low-energy refiner-based method. Details of the production method are found elsewhere (Bilodeau and Paradis 2018). This suspension contained 3 wt.% CNF solids. The fine content of the CNF suspension was measured by a Morfi Analyzer (Techpap SAS, France) to be 90% fines i.e., 90% of the fibers had a length below 200  $\mu\text{m}$ . These CNFs were designated as the standard CNFs. High fines CNFs, which were a 50 min more ground version of the standard CNFs in a super masscolloider (Masuko Sangyo, Model: MKCA6-2/, Kawaguchi, Japan), had a 97.4% fines content. The further details of these two types of CNFs are also available in the work of Ghasemi et al (2017).

### Optical microscopy for fiber dimensions

To observe cellulose nanofibers at the micro-level, an AmScope<sup>TM</sup> (ME520TA, Irvine, CA) optical microscope was used. Very dilute ( $\sim 0.01$  wt.%) suspensions of the two CNFs types were prepared and sonicated for 1 min to make the suspension homogeneous and avoid agglomeration of fibers. Then a very small drop ( $\sim 0.05$  mL) was dropped onto a clean microscope glass slide and dried in air. A  $20\times$  objective was used to capture the image of those dried fibers. Finally, ImageJ (NIH, USA) software was used to measure the fiber dimensions of at least 50 fibrils from the two types of CNFs evaluated here.

### Atomic force and transmission electron microscopy

Smaller scale morphological characteristics of the CNFs and films were evaluated by atomic force microscopy (AFM) and transmission electron microscopy (TEM). The AFM analysis was done using a benchtop ezAFM atomic force microscope (Nano Magnetism Instruments, Oxford, UK). For fibers, the same suspensions as in the optical microscopy ( $\sim 0.01$  wt.%) were used. A single drop ( $\sim 0.05$  mL) from each suspension was placed on a small piece ( $\sim 1\text{ cm} \times 1\text{ cm}$ ) of glass slide that was attached to the magnetic mounting discs with a double-sided tape and dried in air in room conditions. For films, a piece with the dimensions around  $5\text{ mm} \times 5\text{ mm}$  was cut and placed on the mounting

disc directly. A dynamic scanning tapping mode was used to scan an area of  $10\ \mu\text{m} \times 10\ \mu\text{m}$  for dried fibers and films. TEM analysis was done using a Philips/FEI CM10 TEM (Hillsboro, OR). A very dilute suspension of each material ( $\sim 0.01\ \text{wt.}\%$ ) was dropped on a glow-discharged carbon-coated grid and negatively stained with 2% uranyl acetate in water to enhance the contrast.

### Film preparation

The film preparation process slightly varied based on the drying process of the film. The target basis weight for each film was 60 g per square meter (gsm). A 0.5% concentration suspension was prepared for all cases except for casting. For casting, the suspension concentration was 1% so that it could not overflow from a petri dish at a usual size ( $100 \times 15\ \text{mm}$ ) and still obtain the desired basis weight. The suspensions were sonicated for two minutes with a Branson 450 Sonifier (Ultrasonics Corporation, Danbury, CN, USA). Then a thorough mixing to remove bubbles was performed for 1 min using a planetary mixture (Thinky 310, Thinky Corporation, Tokyo, Japan) at 2000 rpm with a subsequent defoaming step for 45 s at 2200 rpm. For the casting purpose, the suspension was gently poured into a petri dish of the mentioned size and slightly shaken to spread uniformly over the Petri dish and kept in a fume hood for 48 h to dry in the air. For other drying processes, the suspension was filtered in a vacuum filtration apparatus maintaining a suction pressure of 254 mm (Hg). For the filtration purpose, Whatman Grade 5 ( $2.5\ \mu\text{m}$  pore size) qualitative filter papers were used. For each film preparation, two filter papers were used on the Buchner funnel to avoid the circular dots that otherwise appeared from the gaps in the funnel where local vacuum pressure is high. The filtration process took around 4 min and was terminated when the interval between two drops falling was at least 20 s.

Once the filtration was complete, the lower filter paper was removed before drying. For oven drying, each film (with the filter paper) was placed on top of a steel plate and then a polyvinyl chloride (PVC) ring with a 10 cm inner diameter was placed on top of the film with another steel plate on top of the ring with a load  $\sim 200\ \text{g}$ . Then the entire setup was kept in an oven for 6 h at  $65\ ^\circ\text{C}$ . For heat gun drying, the setup was almost similar to that for the oven drying, except

that the top steel plate was removed and the PVC ring was clamped from the side. A heat gun (DeWALT, D26960, Baltimore, MD) with a flow rate  $1.2 \pm 0.1\ \text{m/s}$  and a temperature of  $65\ ^\circ\text{C}$  was used to dry the film for 20 min. For hot pressing, the film with an additional new filter paper on top was placed in between two steel plates. Then the entire setup was dried for 10 min between two hot press platens at  $120\ ^\circ\text{C}$  under minimum pressure i.e., the gauge dial was kept at zero with enough pressure only to keep the press closed. The entire wet film setup before drying is shown in Fig. S1. The hot press-assisted compaction for all types of films was performed as shown in Fig. 1 at  $120\ ^\circ\text{C}$  and 1.1 MPa for 10 min.

### Density and porosity of films

For density measurement, films were first conditioned at 50% relative humidity and  $23\ ^\circ\text{C}$  temperature. A circle with a 6.5 cm diameter was cut from all films and then thicknesses from ten random points were measured with a micrometer at 0.001 mm accuracy for each film. The average thickness was considered as the thickness of the overall film for volume calculation. Then the weight of each circle was recorded and divided by the volume to obtain the density. At least the density of three samples from each type of film was measured and recorded with average and standard deviation. For apparent porosity measurement, a formula (Eq. 1) based on film density and cellulose fiber density ( $\rho_c = 1.5\ \text{g/cm}^3$ ) was used (Hossen et al. 2020b).

$$\text{Porosity (\%)} = \frac{\rho_c - \rho_f}{\rho_c} \times 100 \quad (1)$$

### Surface roughness and surface free energy analysis

Along with nano-level surface roughness from AFM, we also used the TAPPI T538 (Technical Association of the Pulp and Paper Industry 1996a) method with Sheffield air leakage measurement instrument (The Sheffield Corporation, Dayton, OH) to measure the degree of roughness on a relative scale. In brief, the instrument and method principle is to flow air between a ring-shaped metal measuring head, which rests on the film's top surface to impart pressure on it, and the top surface of the film. The bottom surface of the film is supported on a flat glass surface. The air leakage

flow rate from the surface of the film is converted to an arbitrary unit, named as Sheffield Unit (SU) that ranges from 0 to approximately 445 SU, where 0 indicates the smoothest surface and 445 indicates the roughest one. To understand the surface properties of films, a double sessile-drop contact angle measurement was performed using a mobile surface analyzer (Kruss, Hamburg, Germany). Two drops of 1  $\mu\text{L}$  each from deionized water (polar probe) and diiodomethane (non-polar probe) were released on the surface of the film and then contact angles were measured just after 1 s of drop falling. From the contact angles of the polar probe and non-polar probe, surface free energy was calculated using Owens, Wendt, Rabel and Kaelble (OWRK) formula (Owens and Wendt 1969). At least 10 measurements were taken for each type of film for average and standard deviation calculation.

#### Transparency of films

For qualitative transparency of films, a University of Maine logo was affixed on one side of a microscopic slide and then a portion of a film (same size as the slide) was placed on the other side of the slide and clipped. Photographs of each type of film were captured and presented together for visual comparison. For the quantitative purpose, a Beckman DU 7500 UV–Visible spectrophotometer (Beckman Coulter, CA, USA) was used to measure the light absorbance of films in the visible region (400–800 nm) using air as the reference. A plastic sample holder was 3D printed with a 1 cm  $\times$  2 cm hole and used to hold the film samples in place. Finally, the transmittance was calculated using the formula  $\text{Transmittance (\%)} = \text{antilog (2-absorbance)}$ .

#### X-ray diffraction

X-ray diffraction (XRD) was used to compare the relative crystallinity of fibers in different films. A PANalytical X'Pert Pro (Royston, UK) XRD instrument was used to scan the films from  $10^\circ 2\theta$  to  $40^\circ 2\theta$  at 45 kV and 40 mA. The radiation source was nickel filtered Cu  $K\alpha$  with a wavelength of 1.54  $\text{\AA}$ . The crystallinity index (CI) of films was calculated based on Segal's formula (Segal et al. 1959).

$$\text{CI (\%)} = \frac{I_{200} - I_{am}}{I_{200}} \quad (2)$$

where  $I_{200}$  denotes the intensity (in arbitrary unit) of the crystalline peak from the (200) plane and  $I_{am}$  is the intensity of the minimum between two major peaks (around  $18^\circ 2\theta$ ) presenting the amorphous portion.

#### Tensile testing

Tensile strength, strain at break, and modulus was evaluated for all prepared films with an Instron 5942 Universal Testing Machine (Instron, MA, USA) with a 500 N load cell. All tested films were cut into 50 mm  $\times$  10 mm specimens. Then all specimens were conditioned at 50% relative humidity and  $23^\circ\text{C}$  for 24 h. The actual gauge length for testing was 20 mm. Then the specimens were tested at a displacement rate of 2 mm/min. At least five specimens from each type of film were tested for the purpose of statistical analysis.

#### Scanning electron microscopy

To evaluate the internal structure of films, a scanning electron microscope (SEM) (Nvision 40, Zeiss, Germany) was used at various magnifications. Before taking images, all samples were coated with a 4 nm layer of Au/Pd using a sputter coater. For cross-sectional images of films, the films were freeze fractured in liquid nitrogen. All films were placed on metal stubs with carbon tapes. The voltage was kept at 3 kV and the working distance was in the range of 11 mm to 15 mm.

#### Oil barrier test

All prepared films were tested for the oil barrier property with standard 'kit test' following the TAPPI T559cm-12 protocol (Technical Association of the Pulp and Paper Industry 1996b). In short, the process involves dropping solutions of different kit numbers (1 to 12) separately on each film from a 13 mm height and then wiping the surface off after 15 s with a cotton ball. The highest kit number at which a dark spot was not observed after cleaning was considered as the kit number of that specific film. The test was replicated for three times at least on each film type.

### Water vapor transmission rate

Water vapor transmission rate (WVTR) was measured following the standard procedure of ASTM E96/E96M-16. To summarize the process, each film was cut into a circular shape of 65 mm. About 50 g of water was poured into a Mason jar (Rubbermaid Incorporated, GA, USA) and the circular film was placed on the top of the jar. A silicone rubber and metal screw cap were used to seal and hold the film in place. The weight of the whole jar with the film was recorded before placing it in an environmental chamber at 23 °C and 50% relative humidity. After conditioning for 24 h, the weight of the jar was recorded again. The difference of weight before and after conditioning ( $\Delta_{mass}$ ) denotes the amount of water vapor transmitted through the film. Then WVTR can be calculated using Eq. 3

$$WVTR \left( \frac{g}{m^2 \cdot day} \right) = \frac{\Delta_{mass}}{\pi r^2 \cdot day} \quad (3)$$

where  $r$  indicates the radius of the film. Water vapor permeability (WVP), which is independent of sample thickness, can be calculated using Eq. (4).

$$WVP \left( \frac{g \cdot mm}{day \cdot kPa \cdot m^2} \right) = WVTR \times \frac{Thickness}{P_{(saturated)} \times \Delta_{RH\%}} \times 100 \quad (4)$$

where  $P_{(saturated)}$  indicates the saturated vapor pressure of water at 23 °C (2.81 kPa) and  $\Delta_{RH\%}$  indicates the difference of relative humidity inside (100%) and outside of the jar (50%).

### Oxygen transmission rate and crack-folding behavior

Oxygen transmission rate (OTR) and oxygen permeability of films were measured following ASTM D3985-17 standard with an OX-TRAN 2/22 OTR Analyzer (MOCON, MN). The film was placed in a designated cell and conditioned for 6 h with a gas mixture of 96% N<sub>2</sub> and 4% H<sub>2</sub> (carrier gas) containing water vapor to make the relative humidity at 50% or 80%. The testing area of each film was 5.64 cm<sup>2</sup>. The test duration varied as the test was continued until a transmission rate was converged upon. The tests were

terminated when the difference between the last measurement and the one from 5 cycles before was less than 1%. Oxygen permeability value was obtained by multiplying the OTR value by the thickness. For the crack resistance test, a standard CNF film dried in hot press was selected as a representative for all CNF films. The first crack was made by folding the film at 180° and then applying a load of 2.5 kg for 10 min as shown in Fig. S2a. The second crack was made in two steps. The first step was the same as the crack in the first film and then in the second step the film was folded again at 180° with the same load and time to make a cross at the center Fig. S2b.

### Statistical analysis

Three-way analysis of variance (ANOVA) was performed for three independent variables (type of CNFs, drying method and hot-press compaction) to understand the main effects and interaction effects of the three independent variables on mechanical and barrier properties. Also, Duncan's post hoc analysis was conducted to classify drying methods based on their group means. All statistical analyses were run in IBM SPSS Statistics 27 (IBM Corporation) with a level of significance of 0.05.

## Results and discussion

### Morphology of fibers

CNFs are mainly defibrillated from cellulose pulp; defibrillation occurs when shear forces are applied on fibers. Different characterization techniques are applied together to understand the fiber morphology for CNFs and other lignocellulosic materials. Here we applied three different-scale characterizations by optical microscope, AFM and TEM. The optical micrographs of the two types of fibers as shown in Fig. 2a, b were used to determine their width. The standard CNFs and high fine CNFs had an average micron-level width of  $1.4 \pm 0.38 \mu\text{m}$  and  $0.91 \pm 0.23 \mu\text{m}$ , respectively. The width of fibers measured from AFM images, as shown in Fig. 2c, d was found to be  $249 \pm 107 \text{ nm}$  and  $239 \pm 62 \text{ nm}$  for the standard and high fines CNFs, respectively. On the other hand, TEM image analysis from Fig. 2e, f showed the diameter of standard CNF film as

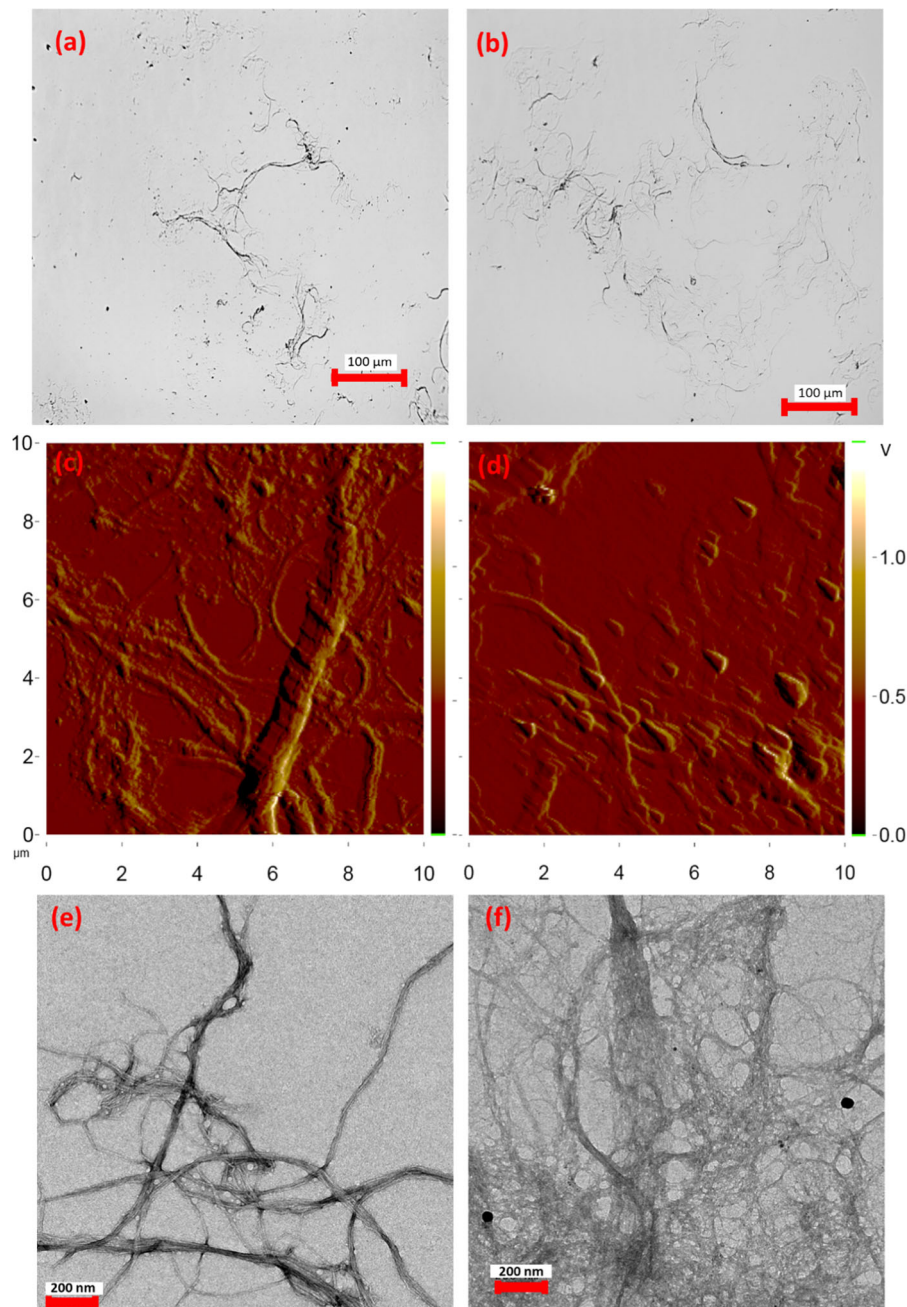


**Fig. 2** Optical micrograph of standard CNFs (a) and high fines CNFs (b), AFM amplitude image of standard CNFs (c) as well as high fines CNFs (d) and TEM images of standard CNFs (e) and high fines CNFs (f)

$37 \pm 15$  nm and that of the high fine CNFs as  $13 \pm 6$  nm. The difference in diameter by different characterization technique was also observed in other reports (Kelly et al. 2021) and can be attributed to the tip broadening effect in AFM or simply the natural variability of the materials. The most dominant

difference was seen in terms of roughness as determined by AFM and shown in Fig. 2c, d. The average roughness of the standard CNFs was  $133 \pm 69$  nm. For high fine CNFs, it was significantly lower ( $62 \pm 26$  nm). From the data, it is also clear that the high fines CNFs had a narrower size distribution than



the standard CNF. The relatively lower width and roughness of the high fine CNFs were due to the additional grinding process in the super masscolloider that resulted in more shear force and defibrillation compared to the standard CNF film (Amini et al. 2020). From the optical micrographs of the high fines CNFs, the finer defibrillated fibrils can be easily seen.

### Density and porosity of films

Film density is one of the most important parameters that give an insight into the properties of the film. Previous studies showed that the mechanical properties of a cellulose nanofibril film are density-driven, rather than governed by the fines content (Amini et al. 2020) or thickness of the film (El Awad Azrak et al. 2019). Statistical analysis showed that the types of fibers, drying methods and hot-press compaction significantly influenced the density. Here in our case, the high fines CNFs films showed on average 10% higher density than standard CNF films (Fig. 3a, b). This observation of a higher density of films with a higher degree of fibrillation complies with the studies of other researchers (Amini et al. 2020; Wakabayashi et al. 2020). The Duncan Post hoc test classified the drying methods into three groups based on the output variable density. Oven-dried films had the lowest density whereas cast films, on average, showed 7.1% higher density while the rest of the drying methods brought about densities in between the two. However, the interaction effects of drying methods with CNF types as well as hot press compaction were also statistically significant. As a result, it is difficult to consider the density in terms of drying methods ignoring other variables. For instance, the standard CNF films prepared by casting showed similar density to those made by hot press drying, but in case of the high fine CNFs films, the cast films showed the highest density. In addition, hot press compaction of the dried films increased the density by 11% denoting that this process contributed the most to increase the density of CNF films. Interestingly, the hot press compaction turned the density into almost similar values irrespective of the drying techniques. Different drying techniques are expected to give different internal structures and free spaces to the films, which is the reason for the different density values of the films. However, the hot press compaction changed the density based on the level of free spaces in a film.

For example, for oven dried films which had the lowest density i.e., more free spaces, hot press compaction increased the density by 17%. In contrast, hot-pressed films had higher density i.e., the film had already lower free spaces, and therefore hot press compaction only improved the density by 6%. The porosity has an opposite relationship with the density i.e., the denser the film the less porous it will be. As expected, high fine CNFs film had lower porosity than standard CNF films as shown in Fig. S3. Similarly, hot press compaction also significantly decreased the porosity as the thermal compression increased the density.

### Transparency of the films

Qualitative transparency of the films is shown in Fig. 4. From this figure, it is quite clear that the films dried with the hot press are less transparent than cast films which are, in turn, less transparent than those made by oven drying and heat gun drying. The UV–vis transmittance, as shown in Fig. 3c, d shows a similar trend. Based on the UV–Vis data, the highest transparency was shown by oven-dried films. Heat gun drying showed almost close transparency to oven drying, but the lowest transparency was observed for films dried by hot press and air. In general, highly densified films are expected to have high transmittance because of the presence of relatively small amount of air pockets which cause the light scattering inside the film (Hsieh et al. 2017). Following this rule, high fine CNFs films showed 54% higher transmittance than standard CNF films at 600 nm wavelength as they have higher density and less porosity than standard CNF films. However, in terms of drying methods, the effect of density on transparency was not found to be the controlling factor as relatively dense air-dried and hot-pressed films showed lower transparency. Lower transparency in this case was most likely controlled by the surface properties instead of bulk properties. For air-dried films, the surface roughness was probably contributing to the lower transmittance. For polymeric films, the surface roughness causes extra light reflection and scattering which eventually reduces the transmittance (Lin et al. 2007). As the Sheffield roughness values, listed in Table 1, were higher for air-dried films, their transmittance was mostly affected by the rough surface. On the other hand, the lowest transmittance of hot-pressed films can be attributed to scattering caused by the hanging fibers on the surface

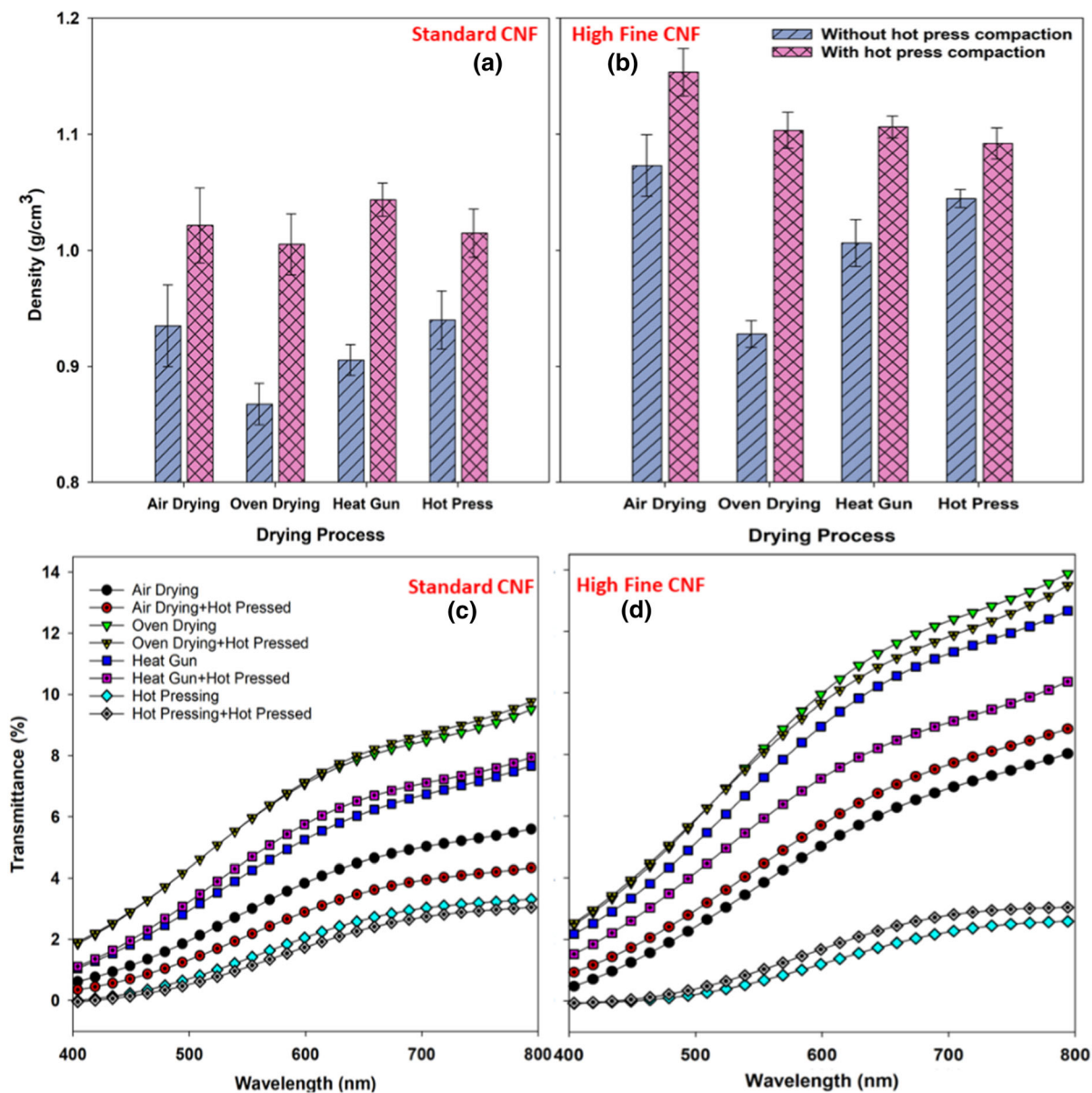


**Fig. 3** Density of standard CNF (a) and high fines CNF film (b). UV–Vis graphs of standard CNF (c) and high fines CNF (d) film

of the films and heat treatment. Nogi et al (2009) prepared a translucent cellulose nanofiber film, which was then converted into a completely transparent film with simple polishing with Emery paper and thus concluded that transparency of the cellulose nanofiber film can also be affected by light scattering from the loosely held fibers on the surface of the films. Here in our case, we used filter paper on both sides of wet films during hot press drying. Nanofibrils on the surface of the wet film can form adhesion with the fibers on the

surface of filter paper and this adhesion is further induced by the pressing. An SEM image of a dried film's surface which was in contact with the filter paper is presented in Fig. S4. From the image, hanging fibers which were formed during the detachment of the filter paper from the film are seen. Those fibers could have caused light scattering from both sides of hot-pressed films. As a result, hot-pressed films were less transparent than those prepared by other drying methods. Besides this effect, the high temperature

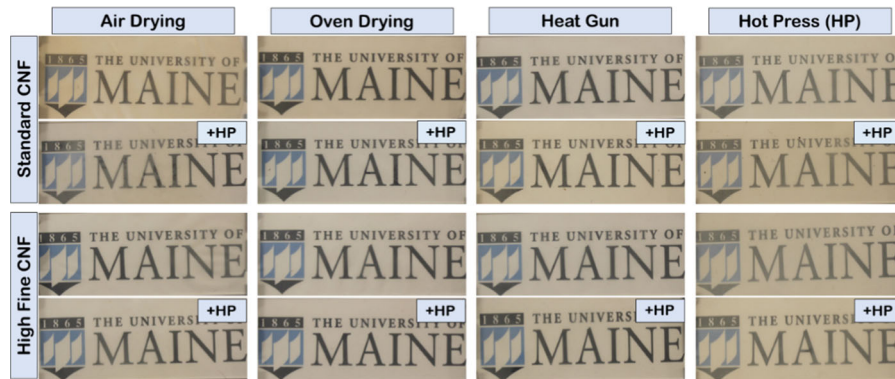


**Fig. 4** Qualitative transparency of all prepared films on the logo of University of Maine. + HP indicates films after hot press compaction. The logo of the University of Maine behind all films was used with the kind permission from the University authority

**Table 1** Average thickness, AFM roughness, Sheffield roughness and surface properties of all films

Drying methods	Film thickness (μm)	AFM roughness (μm)	Roughness (Sheffield)	Surface free energy (mN/m)	Polar (mN/m)	Disperse (mN/m)
<i>Standard CNF film</i>						
Air drying	69 (12)*	0.22 (41)	328 (3)	47.75 (25.88)	10.54 (71.63)	37.22 (12.92)
Air drying + Hot press	58 (9.4)	0.17 (50)	210 (5)	32.16 (27.71)	2.27 (138.8)	29.89 (19.30)
Oven drying	69 (1.4)	0.20 (31)	188 (4)	54.53 (31.89)	23.89 (43.57)	30.64 (22.78)
Oven Drying + Hot Press	54 (8.4)	0.22 (29)	92 (3)	54.10 (14.97)	22.2 (21.76)	31.89 (10.22)
Heat Gun	64 (2.7)	0.28 (47)	133 (2)	52.02 (22.41)	22.44 (29.72)	29.58 (16.87)
Heat gun + Hot press	56 (0.3)	0.22 (65)	75 (7)	50.54 (29.01)	20.25 (46.67)	30.29 (17.20)
Hot press	58 (6.6)	0.23 (35)	193 (2)	67.42 (14.25)	33.76 (15.97)	33.66 (12.54)
Hot press + Hot press	56 (11)	0.28 (31)	100 (0)	58.97 (14.72)	26.28 (19.44)	32.69 (10.92)
<i>High fines CNF film</i>						
Air drying	68 (6.2)	0.32 (52)	295 (2)	54.50 (19.61)	18.15 (39.06)	36.35(9.90)
Air drying + Hot press	62 (3.4)	0.13 (47)	240 (7)	50.00 (14.10)	10.97 (34.82)	39.02 (8.28)
Oven drying	73 (4.1)	0.22 (34)	230 (4)	61.23 (13.10)	26.95 (16.22)	34.27 (10.65)
Oven drying + Hot press	62 (3.2)	0.27 (47)	83 (7)	51.10 (10.08)	20.1 (15.27)	31 (6.7)
Heat gun	71 (6.0)	0.19 (35)	230 (4)	57.03 (29.35)	23.95 (44.22)	33.08 (18.59)
Heat gun + Hot press	61 (1.9)	0.32 (43)	64 (9)	46.19 (26.00)	17.52 (47.83)	28.67 (12.66)
Hot press	63 (3.5)	0.19 (35)	95 (5)	70.74 (7.85)	39.06 (7.83)	31.68 (7.86)
Hot press + Hot press	60 (2.4)	0.17 (36)	67 (4)	57.51 (12.99)	30.79 (25.37)	30.01 (14.30)

\*Values in parentheses indicate coefficients of variations (%)

treatment of the hot-pressed films could possibly make them susceptible to the thermal oxidation which could be responsible for the relatively yellowish appearance of the films and lower transmittance as well (Abral et al. 2020).

### Surface morphology and roughness of films

The AFM amplitude images for all types of films are shown in Fig. S5 to observe any difference in surface morphology. However, no trend or distinct pattern was observed for these images mostly because of the small scanning area ( $10\ \mu\text{m} \times 10\ \mu\text{m}$ ) which is not able to capture the entire variability. As the fiber size distribution is quite random for CNFs, some films, e.g., the standard oven-dried film with hot press compaction and high fines heat-gun dried films, showed the presence of larger width fibers, which are not related to film drying methods at all. To determine the nano-level surface roughness of the film, we used AFM topography images and the values are listed in Table 1. Only drying methods showed a statistically significant effect on the surface roughness of the films. On average, cast films showed  $0.25 \pm 0.01\ \mu\text{m}$  roughness, which is the highest among all drying methods. The reason can be attributed to the free and uneven orientation of fibers on the surface during air drying of casted suspensions. However, after hot press compaction of dried cast films, the roughness reduced by 25% for standard CNF films and 58% for high fine CNFs films.

Although nano-level (smaller than 100 nm) roughness did not seem to be improved for any of cases after hot press compaction, our visual observation showed the smoothing of surface in every case. The macro-level (mm scale) roughness on the films appeared either from the roughness of the filter papers during filtration, which was eventually retained on the film after drying or waviness created during the air drying of casted films. Therefore, we employed the air leakage method, which is widely used in the paper industry, to determine the surface roughness. The Sheffield roughness values of all films are presented in Table 1. Statistical analysis showed that the high fines CNFs film had 18% lower roughness than the standard CNF films in SU. However, this reduction in roughness by hot-press drying is only true for macro-level observation, which may not be true for micro/nano-level roughness. In all cases, hot press compaction

significantly reduced the roughness of all films. For example, oven drying and heat gun assisted drying of high fines CNF made a very rough surface of 230 SU which decreased by 64% and 72% after hot press compaction. Similar to nano-level roughness, cast films without compaction hot pressing showed the highest roughness in the Sheffield test.

### Surface free energy

The surface contact angle and surface free energy of all prepared films were determined to have a deeper understanding of their surface properties. CNF films' surfaces are, in general, hydrophilic due to the hydroxyl groups present in the fibers. In Fig. 5a, b the water contact angles of standard CNF films and high fine CNFs films are presented, respectively. Cast films showed a higher water contact angle, which indicates that these films are more hydrophobic compared to films made through other drying methods. The reason for the higher water contact angle can be related to the roughness of cast film, as the chemistry for all CNF films is the same. According to Wenzel's theory, a hydrophilic material (water contact angle  $< 90^\circ$ ) will be more hydrophilic when micron level ( $\sim 100$  to  $1000\ \mu\text{m}$ ) roughness of the surface can be increased i.e., if two hydrophilic films with the same chemistry have two different degrees of roughness, the smoother one will be less hydrophilic (Wenzel 2015). Although there is no evidence from AFM roughness value that cast films had less roughness than other films as AFM detected only nano-level roughness within a very small ( $10\ \mu \times 10\ \mu$ ) scanning area, contact angle values suggests that cast film may have less micron level roughness compared to films made through other drying methods. On the other hand, hot press compaction, in general, tends to increase water contact angle. Therefore, we can conclude that hot press compaction increases the hydrophobicity of the surfaces and this hydrophobicity can also be related to less roughness of hot-pressed film at the micron level. In terms of the fines content of the fibers, no significant difference was found. Previously, Amini et al. (2020) reported that hydrophobicity of CNF films increased from a fine content of 50% to 100%. However, in our case, the difference in fines content between the two samples was not that high, which might be the reason for no significant difference.

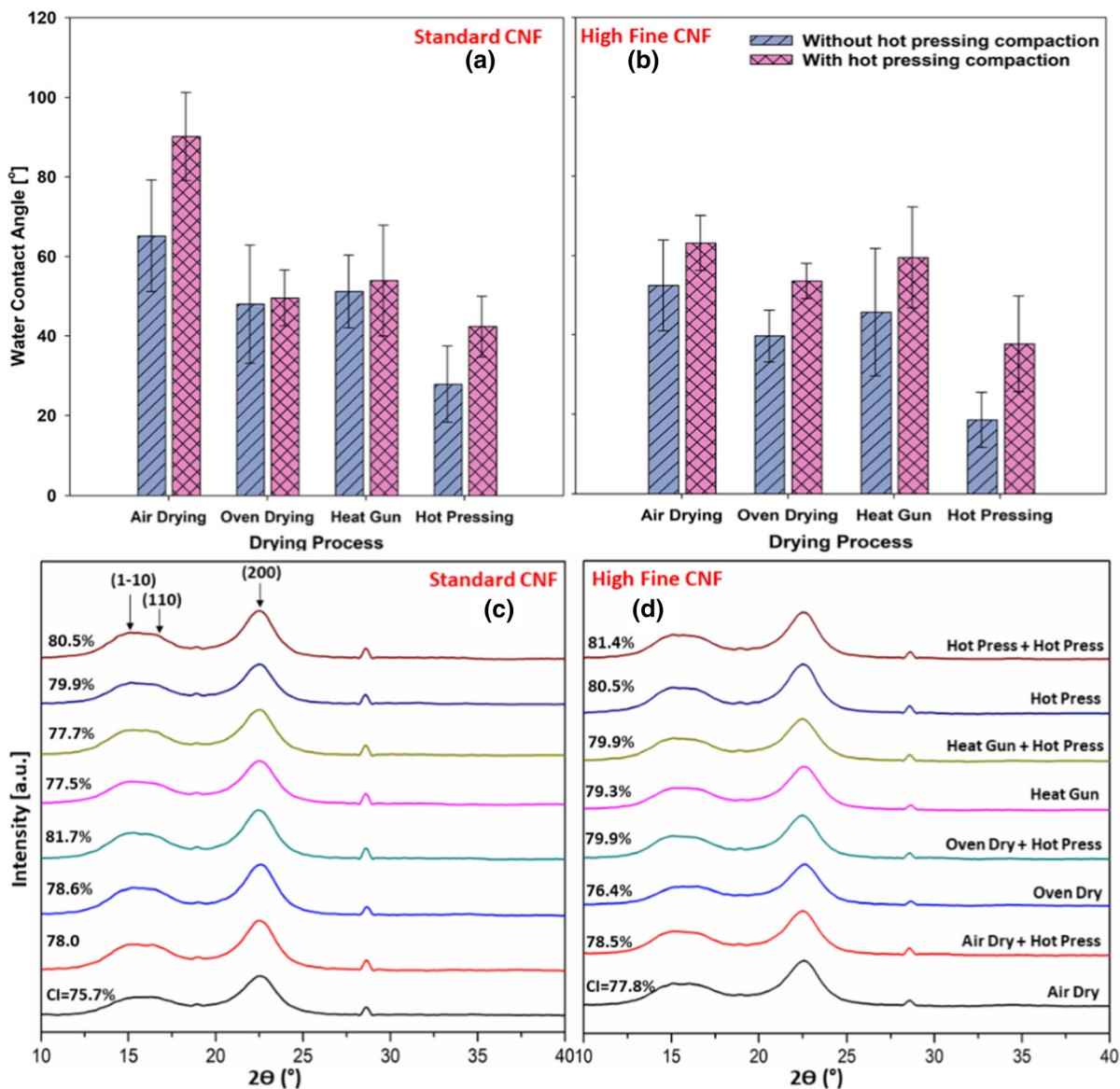


**Fig. 5** Water contact angle of standard CNF (a) and high fines CNF (b) film. XRD graphs along with crystallinity index (CI) of standard CNF (c) and high fines CNF (d) film

The crystallinity of the films

The crystallinity of cellulose nanofibril films has already shown to influence the mechanical properties of the films (Qing et al. 2015). In general, cellulose nanofibrils films are randomly oriented in films unless any special treatment is performed to make them aligned (Uddin et al. 2011; Sehaqui et al. 2012). From the XRD graphs of standard CNFs and high fines CNFs as shown in Fig. 5c, d the peaks in between 15

and 16.5° corresponds to (1–10) and (110) lattice planes which are characteristic peaks of cellulose observed by many other researchers (French 2014; Hafez et al. 2020). The most dominant peak in terms of intensity was found around 22.5° which corresponds to (200) lattice diffraction. The crystallinity indices (CI) for all films were in the range of 75–82%. Cast films showed the lowest CI whereas hot-pressed films showed the highest CI value, which suggest that the casting process gives more random orientation of

fibers during drying whereas hot pressing gives more crystalline zone during drying. This observation can be relevant to mechanical and barrier properties discussed at a later portion of this paper. Another significant observation from XRD data is that hot press compaction on dried films increased the CI in all cases. This is not an observation that happened by chance, rather a number of research findings showed the same phenomenon and related this result to the reorientation of fibers caused by heat and pressure (Kumar and Kothari 1999; Qing et al. 2015).

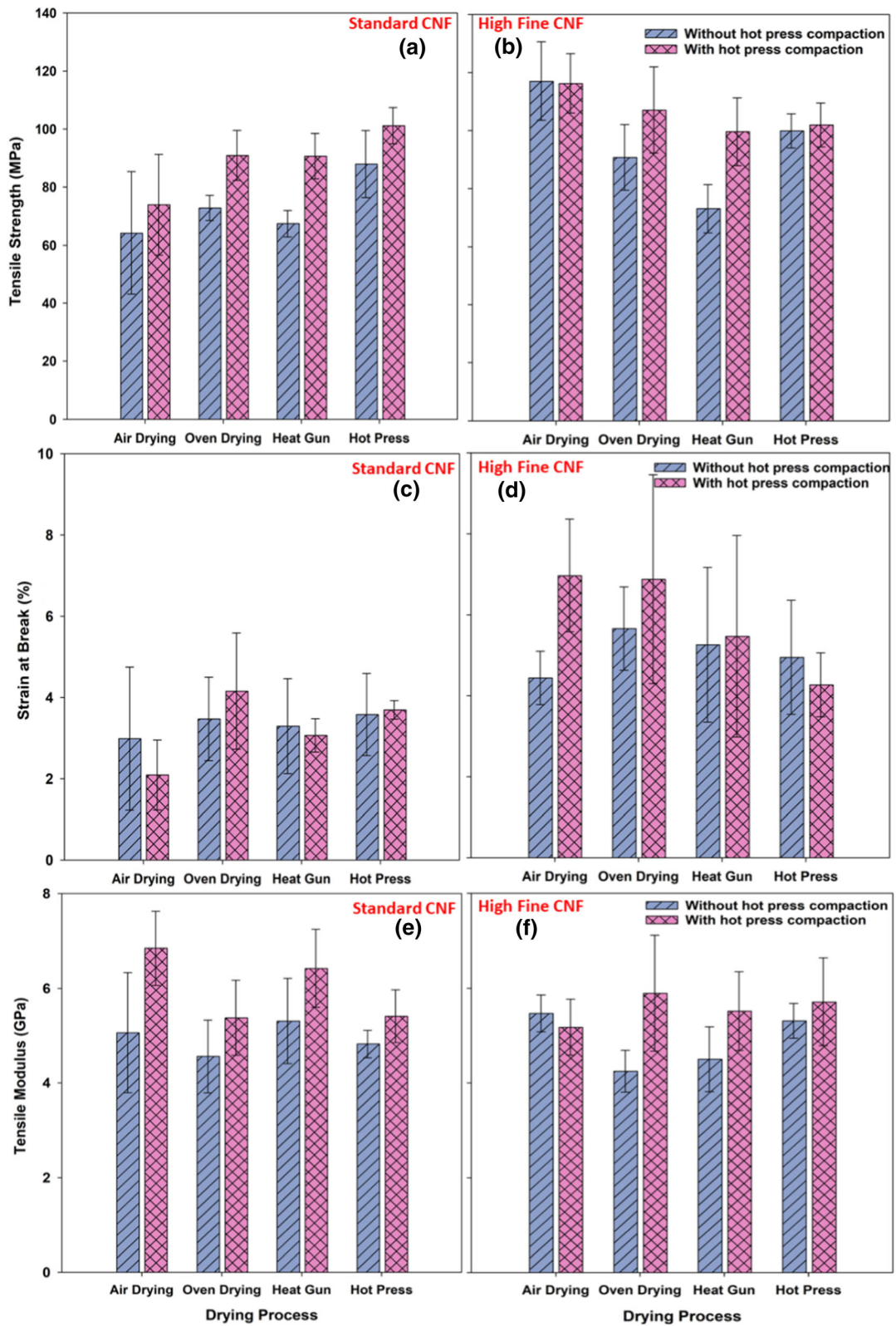
### Mechanical properties of the films

Mechanical properties of CNF films are important for many applications, especially where lightweight but high strength materials are desired (Hossen et al. 2018; Guan et al. 2020). All tensile test results (strength, strain at break, and modulus) are shown in Fig. 6 along with a representative stress–strain curves from each sample in Fig. S6. Clearly, different drying methods and morphologies make different materials from wet cellulose nanofibril hydrogels in terms of strength. Qing et al (2015) showed that freeze-drying and casting generated low strength cellulose nanofiber films. Here in our case, Duncan's post hoc test classified the drying methods into three groups- high strength with an average of 98.8 MPa for hot pressing, medium strength with an average 89.9 MPa and 91.3 MPa respectively for oven drying and heat gun assisted drying and finally low strength materials with an average of 83.4 MPa for casting. However, this classification is more considerable for standard CNF films as the interaction effect of drying method and type of CNF was also statistically significant. Cast high fine CNFs films had the highest average strength among all films and it was 77.3% higher than the average strength of the cast standard CNF films. Therefore, it is reasonable to conclude that the higher degree of fibrillation of the fibers will be more advantageous in terms of strength if the preparation process is casting. The difference observed in the strength could have also been caused by the processing techniques. For casting, the nanofibers are driven by Brownian motion and form networks while drying progresses. On the other hand, most of the networks are formed before the drying starts during filtration process. As a result, the difference in properties is expected. Fein et al. reported the higher strength value

of filtered films than casted films at the same density which was similar to our observation (Fein et al. 2021a). Among the filtered films, hot-pressed films showed the highest strength because of the strong hydrogen bonding induced by high temperature and pressure (Österberg et al. 2013).

In general, the use of high fine CNFs films increased the average strength of the films by 24.2% compared to that for the standard CNF films. The strength development by more fibrillated structure was expected because more fibrillated structures can pack better. An important consideration is that the porosity reduction will occur at the core, not at the surface. Refined CNFs at 90% fines content are dense enough at the top and bottom surfaces; further fibrillation will reduce the porosity at the core layer (Fein et al. 2021a). Finally, the hot press compaction significantly increased the tensile strength. On average, the increase in tensile strength caused by hot press compaction was 13.1%. This increase is caused by the lower porosity as well as improved consolidation of fibers induced by the thermal compression as shown by others (Österberg et al. 2013; El Awad Azrak et al. 2019).

In terms of tensile strain, only the degree of fibrillation showed a statistically significant effect. The high fine CNFs films, on average, showed 66.6% higher strain than the standard CNF films. A similar observation for the increase of strain with the increase of the degree of fibrillation was also reported by Wakabayashi et al (2020) for 2,2,6,6-tetramethylpiperidine-1-oxyl (TEMPO) oxidized CNF films. In terms of tensile modulus, which indicates the stiffness of the film, only the drying method showed a statistically significant effect. Duncan's post hoc test classified casting and heat gun drying as the low modulus drying methods with a mean of 4.76 GPa and 5.09 GPa, respectively and hot pressing and oven drying as high modulus drying methods with a mean of 5.61 GPa and 6.07 GPa, respectively. Although tensile modulus of the hot-pressed films was lower than that of the oven dried films, this lower mean was not statistically significant and also hot pressing was more convenient in terms of processing time and solvent resistivity (Österberg et al. 2013). Therefore, hot pressing can be considered the most convenient drying method to prepare strong and stiff CNF films. Besides the drying method, hot pressing compaction after drying seems to have a positive effect on the CNF film modulus although statistical analysis showed that such



◀ **Fig. 6** Tensile strength (a, b), strain at break (c, d), and modulus (e, f) of standard CNF and high fines CNF films

a difference was not significant. Except for high fine cast films, hot press compaction increased the average modulus. The exception for high fine cast films can be explained by the fact that relatively smaller particles in the high fines CNFs may align themselves along the drying line as a result of the surface tension torque (Mashkour et al. 2014) better than those in the standard CNFs and that alignment can result in a high density film which cannot be further densified with hot press compaction (Chowdhury et al. 2019b). The same reasoning can be used to explain the higher strength and strain at break of high fine air-dried films than standard CNF films. With more fibrillation, surface tension torque helped more for the better compaction of nanofibers, which resulted in a denser film.

To prove the concept that the changes occurring here are not caused by the density, we normalized the tensile strength, strain, and modulus by the density of the corresponding films and then performed ANOVA tests again with these specific mechanical properties. For specific tensile strength, type of CNFs, drying methods as well as hot press compaction all showed statistically significant effects as before. However, for specific tensile strain, the effect of hot-press compaction also showed a statistically significant difference along with type of CNFs. Hot press compaction decreased the specific strain by 17.1%. In the case of specific modulus, type of CNFs and hot-press compaction also showed a significant effect.

#### Oil barrier property

Cellulose nanofiber films are well known for their grease and oil resistance (Tyagi et al. 2019). In our study, all the prepared films, regardless of degrees of fibrillation, drying processes or thermal compression, showed a kit value of '12', which indicates the highest oil and grease resistance. Similar values were also obtained by Tayeb et al. (2020) and Hossain et al. (2021) who coated CNFs or lignin-containing CNFs on paper or wood flour composites, respectively, for per- and polyfluoroalkyl substance (PFAs) free oil repellent food packaging applications. The reason for this high grease barrier property can be attributed to

less porous and more tortuous structure formed by the cellulose nanofiber due to very strong hydrogen bonding between fibers.

#### Water vapor permeability

Cellulose nanomaterials are not exceptionally good in terms of water vapor barrier properties due to their hydrophilic nature (Findenig et al. 2012). Some efforts were already made to improve the water vapor barrier property of cellulose nanomaterials by adding crystalline clay materials or other polymeric materials to their formulations (Tayeb and Tajvidi 2019; Nuruddin et al. 2021). Here we attempted to improve the water vapor barrier property with physical parameters and our results of water vapor permeability of different films are shown in Fig. 7. All three parameters in our study showed a statistically significant effect on water vapor permeability. In general, the high fines CNFs films showed 5.8% lower average permeability than the standard CNF films.

In terms of drying methods, Duncan's post hoc test showed that hot-pressed films had the lowest water vapor permeability with an average of 13.91 g mm/m<sup>2</sup> day kPa compared to all other films. On the other hand, standard cast CNF films showed the highest permeability towards water vapor with an average of 17.20 g mm/m<sup>2</sup> day kPa, respectively. Oven-dried and heat gun dried films showed values in between these with an average 13.91 g mm/m<sup>2</sup> day kPa and 17.20 g mm/m<sup>2</sup> day kPa. To reveal the structural reasons for this result, we investigated the cross-sectional area of standard CNF cast film, oven-dried film and hot-pressed film with a field emission SEM as shown in Fig. 8a–c, respectively. CNF films are well known for their layered structure formation during drying reported by many researchers (Aulin et al. 2010; El Awad Azrak et al. 2019). In our observation, however, this was not entirely true for cast films as we found a combination of lamellar structure and random structure for the cast film. In Fig. 8a, a cross-section of such random zone is shown, and this random zone may cause more diffusion of water vapor than the lamellar zone. Oven-dried and hot-pressed films showed perfect lamellar structure in every portion of the film. However, oven-dried films' layers showed a wavy pattern (Fig. 8b) which resulted in more free spaces between layers and caused higher water vapor permeability. In the hot-pressed films as shown in Fig. 8c,



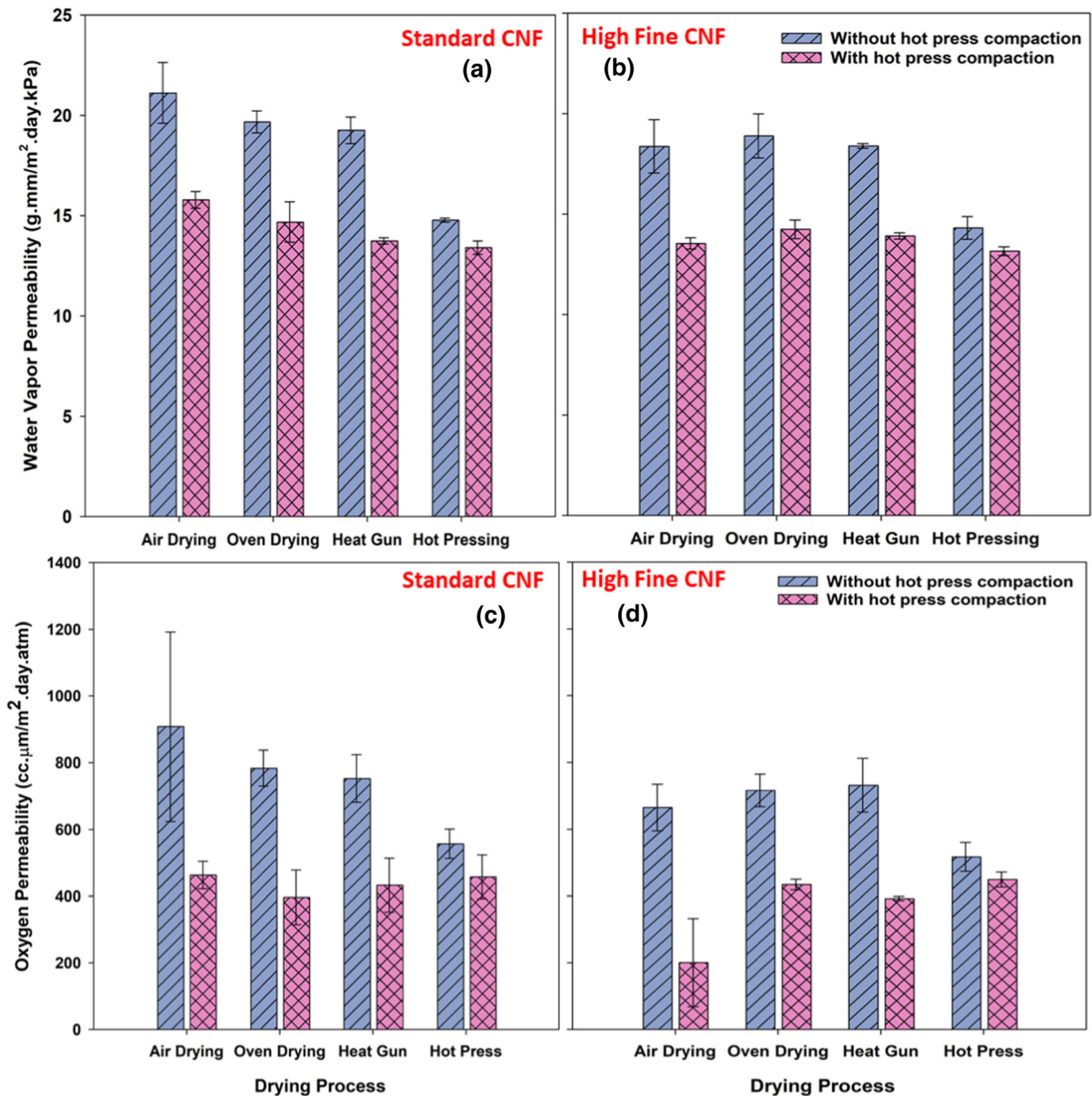


**Fig. 7** Water vapor permeability at 50% relative humidity and 23 °C of standard CNF films (a), high fines CNF film (b) and oxygen permeability at 80% relative humidity of standard CNF films (c) and high fines CNF film (d)

due to the application of pressure, each layer was flat and so the overall structure was more compacted resulting in low water vapor permeability among all drying methods.

The hot-pressed compaction of films also significantly reduced (22.3%) the water vapor permeability. Figure 8d showed the SEM image of oven-dried plus hot-pressed film; the wavy nature of layers is not visible, rather the structure exactly matches of the hot-

pressed film. Therefore, we can conclude that hot press compaction renders the micro-layers in laminates of CNF flat and straight, which eventually leads to less free volume and hence better water vapor barrier property.

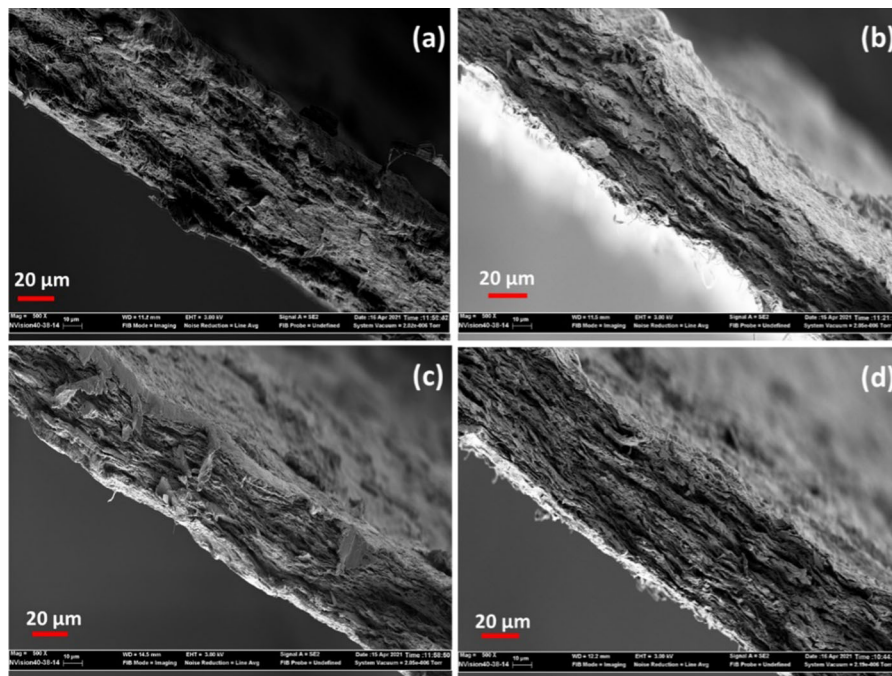


**Fig. 8** SEM images of cross-sections of (a) casted (b) oven-dried, (c) hot pressed, and (d) oven-dried + hot pressed films

### Oxygen barrier and crack resistance

Cellulose nanofibers have excellent oxygen barrier properties at lower relative humidity, which gradually deteriorate at relative humidity higher than 65% due to plasticizing effect of moisture uptake from the environment which works as a medium for oxygen penetration (Nair et al. 2014). The oxygen permeability of all prepared films at 80% relative humidity is shown in Fig. 7c, d. It is evident from the figure that hot pressing resulted in the lowest oxygen permeability compared to all other drying methods. However, statistical analysis showed an insignificant difference between drying processes. This is due to the higher standard deviations between samples as the oxygen permeability is very sensitive to the subtle change of film structure. The largest fluctuation was observed in the oxygen permeability of cast standard CNF film due to the non-uniform formation while drying in air (Shimizu et al. 2014). However, oxygen permeability showed a significant difference with the type of CNFs. High fines CNF films showed 13.6% less oxygen permeability than standard CNF films. With a higher degree of fibrillation, more surface is exposed for hydrogen bonding which results in lower porosity and restricts oxygen passage.

The most significant parameter that changed oxygen permeability is hot press compaction. Hot press compaction on dried films reduced the oxygen permeability by 43%. The reduction of oxygen permeability was also observed in another work by Tayeb et al (2020). The reason for this reduction can also be associated with the change in structure caused by the compaction hot pressing as shown in Fig. 8b, d. Therefore, it can be concluded that the flat and straight deposition of each lamella is an important factor for higher barrier properties that can be attained by direct hot pressing or hot press compaction on dried films. The average value of oxygen permeability after hot press compaction on all types of dried films was found to be 403.2 cc  $\mu\text{m}^2$  day atm, which was a very close value to classify them as high barrier materials (40–400 cc  $\mu\text{m}^2$  day atm) at 80% relative humidity (Wang et al. 2018). A comparison of our obtained mean value with values from other research as well as other natural and petroleum based packaging materials is provided in Table S1.

Along with the oxygen barrier property, another important aspect of packaging materials are their resistance under certain tensions like folding (Tayeb and Tajvidi 2019). Previously Tayeb et al. (2019,2020) showed how cracks at folding affect the

oil and water vapor barrier properties. Here we revealed how CNF films behave in terms of oxygen barrier after fold-cracking. From all 16 categories of films evaluated here, we chose standard CNF films that were dried in the hot press as a representative for fold-cracking behavior. As the oxygen barrier property is very susceptible to pores, we expected to have very high oxygen permeability after folding if cracks did appear. Surprisingly, we obtained the very similar values of oxygen transmission rate before and after a single line fold-cracking. The value of OTR, in this case, was found to be  $10.56 \text{ cc/m}^2 \text{ day}$  at 80% relative humidity, which is comparable to the OTR value before folding ( $9.55 \text{ cc/m}^2 \text{ day}$ ). However, when two crossing fold-lines were made, both samples failed in the OTR testing. The reason for failure was that oxygen transmission was so high (usually  $> 3000 \text{ cc/m}^2 \text{ day}$ ) that the sensor of the machine was saturated by the oxygen and the test was stopped.

To understand the structural change after fold-cracking, we observed the SEM image of the fold line area as presented in Fig. 9a–c. For single-line folding, we did not find any sign of cracks on the surface of the film. To mark the crack zone, we made a small notch with a razor blade on carbon tape in line with the fold line. Still no crack was observed on the film surface as shown in Fig. 9a. Therefore, we can conclude that any visible structural change in the film was not mediated by the single line folding. Later we examined the structure of two crossline folding under SEM. In this case, we found a real crack at the point of the intersection of two lines as shown in Fig. 9b. Also, we saw a slight crack propagation in a line from the crack center. When the second line crossed the first line which was already weak, the crack at the intersection propagated towards the first line. At higher

magnification ( $2000\times$ ), we can see the holes created at the point of intersection in Fig. 9c. Those small holes were large enough for oxygen molecules passage to fail the OTR test.

## Conclusion

In conclusion, drying processes and degree of fibrillation can significantly affect the mechanical and barrier properties of cellulose nanofibril films. Among all drying methods, hot pressing gave the highest mechanical strength as well as the lowest water vapor and oxygen permeability due to better consolidation of layers in the film structures induced by the high pressure and temperature. Along with the drying method, hot pressing compaction on dried films also increased tensile strength by 13% and reduced water vapor and oxygen permeability by 22% and 43%, respectively. SEM images showed hot pressing flattened the layers of CNFs and minimized the free space between two layers. In general, high fines CNF films also showed higher strength and lower water vapor and oxygen permeability than standard CNF film. However, the improved effect of high fines CNFs can be achieved by standard CNFs if hot pressing is used as the drying method and hot press compaction is performed on the dried films. These findings have notable significance in terms of commercialization of CNF films as we may not need to invest money for extra refining, rather a simple thermal compression can generate similar results in terms of strength, water vapor and oxygen permeability even at lower fine contents. Crack resistance behavior in terms of oxygen permeability was also evaluated. A film with a single line folding made at  $180^\circ$  did not show any significant

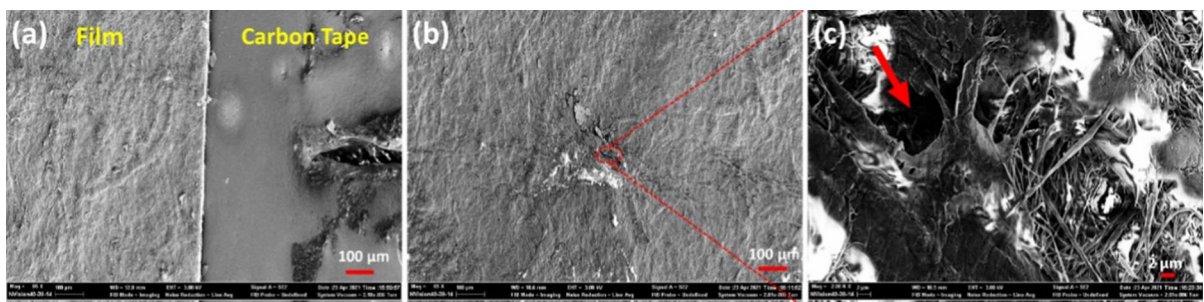


**Fig. 9** SEM images of single-line folded (a) and double-line cross folded (b) films' surface at  $85\times$ . Higher magnification ( $2000\times$ ) of the intersecting point for the double-line cross folded film to see cracks as marked with the red arrow

difference as no crack was practically created in micrometer level. However, double line crossed folding caused the film to fail for over saturation of the oxygen in the sensor as a crack was created at the point of intersection.

**Funding** This work was partially supported through the agreement 19-JV-11111124–062 between the U.S. Forest Service and the University of Maine and by USDA Agricultural Research Service (ARS).

#### Declarations

**Conflict of interest** The authors have no conflict of interests for this article.

**Informed consent** The manuscript was written through contributions of all authors. All authors have given approval to the final version of the manuscript.

**Ethical approval** This study does not involve any human or animal subjects.

#### References

- Abral H, Arikxa J, Mahardika M et al (2020) Effect of heat treatment on thermal resistance, transparency and antimicrobial activity of sonicated ginger cellulose film. *Carbohydr Polym* 240:116287. <https://doi.org/10.1016/j.carbpol.2020.116287>
- Amini E, Hafez I, Tajvidi M, Bousfield DW (2020) Cellulose and lignocellulose nanofibril suspensions and films: a comparison. *Carbohydr Polym* 250:117011. <https://doi.org/10.1016/j.carbpol.2020.117011>
- Aulin C, Gällstedt M, Lindström T (2010) Oxygen and oil barrier properties of microfibrillated cellulose films and coatings. *Cellulose* 17:559–574. <https://doi.org/10.1007/s10570-009-9393-y>
- Bilodeau M, Paradis M (2018) High efficiency production of nanofibrillated cellulose, US Patent No. 9,988,762 B2
- Chowdhury RA, Clarkson C, Montes F et al (2019a) Cellulose nanocrystal (CNC) coatings with controlled anisotropy as high-performance gas barrier films. *ACS Appl Mater Interfaces* 11:1376–1383. <https://doi.org/10.1021/acsami.8b16897>
- Chowdhury RA, Nuruddin M, Clarkson C et al (2019b) Cellulose nanocrystal (CNC) coatings with controlled anisotropy as high-performance gas barrier films. *ACS Appl Mater Interfaces* 11:1376–1383. <https://doi.org/10.1021/acsami.8b16897>
- Du H, Liu W, Zhang M et al (2019) Cellulose nanocrystals and cellulose nanofibrils based hydrogels for biomedical applications. *Carbohydr Polym* 209:130–144. <https://doi.org/10.1016/j.carbpol.2019.01.020>
- El Awad Azrak SM, Clarkson CM, Moon RJ et al (2019) Wet-stacking lamination of multilayer mechanically fibrillated cellulose nanofibril (CNF) sheets with increased mechanical performance for use in high-strength and lightweight structural and packaging applications. *ACS Appl Polym Mater* 1:2525–2534. <https://doi.org/10.1021/acsapm.9b00635>
- Fein K, Bous DW, Gramlich WM (2021a) Processing effects on structure, strength, and barrier properties of refiner-produced cellulose nanofibril layers. *ACS Appl Polym Mater* 3:3666–3678. <https://doi.org/10.1021/acsapm.1c00620>
- Fein K, Bousfield DW, Gramlich WM (2021b) Processing effects on structure, strength, and barrier properties of refiner-produced cellulose nanofibril layers. *ACS Appl Polym Mater* 3:3666–3678. <https://doi.org/10.1021/acsapm.1c00620>
- Findenig G, Leimgruber S, Kargl R et al (2012) Creating water vapor barrier coatings from hydrophilic components. *ACS Appl Mater Interfaces* 4:3199–3206. <https://doi.org/10.1021/am300542h>
- French AD (2014) Idealized powder diffraction patterns for cellulose polymorphs. *Cellulose* 21:885–896. <https://doi.org/10.1007/s10570-013-0030-4>
- Fu T, Moon RJ, Zavattieri P et al (2017) Cellulose nanomaterials as additives for cementitious materials. Woodhead publishing series in composites science and engineering. Woodhead Publishing, Cambridge, pp 455–482
- Ghasemi S, Tajvidi M, Bousfield DW et al (2017) Dry-spun neat cellulose nanofibril filaments: influence of drying temperature and nanofibril structure on filament properties. *Polymers (basel)* 9:392. <https://doi.org/10.3390/polym9090392>
- Ghasemi S, Rahimzadeh-Bajgiran P, Tajvidi M, Shaler SM (2020) Birefringence-based orientation mapping of cellulose nanofibrils in thin films. *Cellulose* 27:677–692. <https://doi.org/10.1007/s10570-019-02821-2>
- Groh KJ, Backhaus T, Carney-Almroth B et al (2019) Overview of known plastic packaging-associated chemicals and their hazards. *Sci Total Environ* 651:3253–3268. <https://doi.org/10.1016/j.scitotenv.2018.10.015>
- Guan QF, Bin YH, Han ZM et al (2020) Lightweight, tough, and sustainable cellulose nanofiber-derived bulk structural materials with low thermal expansion coefficient. *Sci Adv* 6:1–9. <https://doi.org/10.1126/sciadv.aaz1114>
- Hafez I, Amini E, Tajvidi M (2020) The synergy between cellulose nanofibrils and calcium carbonate in a hybrid composite system. *Cellulose* 27:3773–3787. <https://doi.org/10.1007/s10570-020-03032-w>
- Hossain R, Tajvidi M, Bousfield D, Gardner DJ (2021) Multi-layer oil-resistant food serving containers made using cellulose nanofiber coated wood flour composites. *Carbohydr Polym*. <https://doi.org/10.1016/j.carbpol.2021.118221>
- Hossen MR, Dadoo N, Holomakoff DG et al (2018) Wet stable and mechanically robust cellulose nano fibrils (CNF) based hydrogel. *Polymer (guildf)* 151:231–241. <https://doi.org/10.1016/j.polymer.2018.07.016>
- Hossen MR, Talbot MW, Gramlich WM, Mason MD (2020a) Robust nanofibrillated cellulose composite SERS substrate for capillary preconcentration and trace level detection of organic molecules. *Cellulose* 27:10119–10137. <https://doi.org/10.1007/s10570-020-03478-y>

- Hossen MR, Talbot MW, Kennard R et al (2020b) A comparative study of methods for porosity determination of cellulose based porous materials. *Cellulose* 27:6849–6860. <https://doi.org/10.1007/s10570-020-03257-9>
- Hsieh MC, Koga H, Suganuma K, Nogi M (2017) Hazy transparent cellulose nanopaper. *Sci Rep* 7:1–7. <https://doi.org/10.1038/srep41590>
- Kelly PV, Gardner DJ, Gramlich WM (2021) Optimizing lignocellulosic nanofibril dimensions and morphology by mechanical refining for enhanced adhesion. *Carbohydr Polym* 273:118566
- Kumar V, Kothari SH (1999) Effect of compressional force on the crystallinity of directly compressible cellulose excipients. *Int J Pharm* 177:173–182. [https://doi.org/10.1016/S0378-5173\(98\)00340-8](https://doi.org/10.1016/S0378-5173(98)00340-8)
- Lin YJ, Dias P, Chum S et al (2007) Surface roughness and light transmission of biaxially oriented polypropylene films. *Polym Eng Sci* 47:1658–1665. <https://doi.org/10.1002/polb.20850>
- Mashkour M, Kimura T, Kimura F et al (2014) Tunable self-assembly of cellulose nanowhiskers and polyvinyl alcohol chains induced by surface tension torque. *Biomacromol* 15:60–65. <https://doi.org/10.1021/bm401287s>
- Moon RJ, Schueneman GT, Simonsen J (2016) Overview of cellulose nanomaterials, their capabilities and applications. *Jom* 68:2383–2394. <https://doi.org/10.1007/s11837-016-2018-7>
- Nadeem H, Naseri M, Shanmugam K et al (2020) An energy efficient production of high moisture barrier nanocellulose/carboxymethyl cellulose films via spray-deposition technique. *Carbohydr Polym* 250:116911. <https://doi.org/10.1016/j.carbpol.2020.116911>
- Nair SS, Zhu JY, Deng Y, Ragauskas AJ (2014) High performance green barriers based on nanocellulose. *Sustain Chem Process* 2:1–7. <https://doi.org/10.1186/s40508-014-0023-0>
- Nogi M, Iwamoto S, Nakagaito AN, Yano H (2009) Optically transparent nanofiber paper. *Adv Mater* 21:1595–1598. <https://doi.org/10.1002/adma.200803174>
- Nuruddin M, Chowdhury RA, Szeto R et al (2021) Structure – property relationship of cellulose nanocrystal – polyvinyl alcohol thin films for high barrier coating applications. *ACS Appl Mater Interfaces* 13:12472–12482. <https://doi.org/10.1021/acsami.0c21525>
- Österberg M, Vartiainen J, Lucenius J et al (2013) A fast method to produce strong NFC films as a platform for barrier and functional materials. *ACS Appl Mater Interfaces* 5:4640–4647. <https://doi.org/10.1021/am401046x>
- Owens DK, Wendt RC (1969) Estimation of the surface free energy of polymers. *J Appl Polym Sci* 13:1741–1747. <https://doi.org/10.1002/app.1969.070130815>
- Qing Y, Sabo R, Wu Y et al (2015) Self-assembled optically transparent cellulose nanofibril films: effect of nanofibril morphology and drying procedure. *Cellulose* 22:1091–1102. <https://doi.org/10.1007/s10570-015-0563-9>
- Sacui IA, Nieuwendaal RC, Burnett DJ et al (2014) Comparison of the properties of cellulose nanocrystals and cellulose nanofibrils isolated from bacteria, tunicate, and wood processed using acid, enzymatic, mechanical, and oxidative methods. *ACS Appl Mater Interfaces* 6:6127–6138. <https://doi.org/10.1021/am500359f>
- Satam CC, Irvin CW, Lang AW et al (2018) Spray-coated multilayer cellulose nanocrystal - chitin nanofiber films for barrier applications. *ACS Sustain Chem Eng* 6:10637–10644. <https://doi.org/10.1021/acssuschemeng.8b01536>
- Segal L, Creely JJ, Martin AE, Conrad CM (1959) An empirical method for estimating the degree of crystallinity of native cellulose using the X-ray diffractometer. *Text Res J* 29:786–794. <https://doi.org/10.1177/004051755902901003>
- Sehaqui H, Ezekiel Mushi N, Morimune S et al (2012) Cellulose nanofiber orientation in nanopaper and nanocomposites by cold drawing. *ACS Appl Mater Interfaces* 4:1043–1049. <https://doi.org/10.1021/am2016766>
- Shimizu M, Saito T, Fukuzumi H, Isogai A (2014) Hydrophobic, ductile, and transparent nanocellulose films with quaternary alkylammonium carboxylates on nanofibril surfaces. *Biomacromol* 15:4320–4325. <https://doi.org/10.1021/bm501329v>
- Tayeb AH, Tajvidi M (2019) Sustainable barrier system via self-assembly of colloidal montmorillonite and cross-linking resins on nanocellulose interfaces. *ACS Appl Mater Interfaces* 11:1604–1615. <https://doi.org/10.1021/acami.8b16659>
- Tayeb AH, Tajvidi M (2020) Enhancing the oxygen barrier properties of nanocellulose at high humidity: numerical and experimental assessment. *Sustain Chem* 1:198–208. <https://doi.org/10.3390/suschem1030014>
- Tayeb P, Tayeb HA (2019) Nanocellulose applications in sustainable electrochemical and piezoelectric systems: a review. *Carbohydr Polym* 224:115149. <https://doi.org/10.1016/j.carbpol.2019.115149>
- Tayeb AH, Amini E, Ghasemi S, Tajvidi M (2018) Cellulose nanomaterials-binding properties and applications: a review. *Molecules* 23:1–24. <https://doi.org/10.3390/molecules23102684>
- Tayeb AH, Tajvidi M, Bousfield D (2020) Paper-based oil barrier packaging using lignin-containing cellulose nanofibrils. *Molecules*. <https://doi.org/10.3390/molecules25061344>
- Technical Association of the Pulp and Paper Industry (1996a) Test method T 538 om-96: Roughness of paper and paperboard (Sheffield method)
- Technical Association of the Pulp and Paper Industry (1996b) Test Method T 559 cm-12, Grease resistance test for paper and paperboard
- Tyagi P, Lucia LA, Hubbe MA, Pal L (2019) Nanocellulose-based multilayer barrier coatings for gas, oil, and grease resistance. *Carbohydr Polym* 206:281–288. <https://doi.org/10.1016/j.carbpol.2018.10.114>
- Uddin AJ, Araki J, Gotoh Y (2011) Toward “Strong” Green nanocomposites: polyvinyl alcohol reinforced with extremely oriented cellulose whiskers. *Biomacromol* 12:617–624. <https://doi.org/10.1021/bm101280f>
- Wakabayashi M, Fujisawa S, Saito T, Isogai A (2020) Nanocellulose film properties tunable by controlling degree of fibrillation of TEMPO-oxidized cellulose. *Front Chem* 8:1–9. <https://doi.org/10.3389/fchem.2020.00037>

Wang J, Gardner DJ, Stark NM et al (2018) Moisture and oxygen barrier properties of cellulose nanomaterial-based films. *ACS Sustain Chem Eng* 6:49–70. <https://doi.org/10.1021/acssuschemeng.7b03523>

Wang L, Chen C, Wang J et al (2020) Cellulose nanofibrils versus cellulose nanocrystals: Comparison of performance in flexible multilayer films for packaging applications. *Food Packag Shelf Life* 23:100464. <https://doi.org/10.1016/j.fpsl.2020.100464>

Wenzel R (2015) Resistance of solid surfaces to wetting by water. *Ind Eng Chem* 28:988–994. <https://doi.org/10.1021/ie50320a024>

**Publisher's Note** Springer Nature remains neutral with regard to jurisdictional claims in published maps and institutional affiliations.